



HAL
open science

Coupling between surface plasmon modes on metal films

J. Seidel, F.I Baida, L. Bischoff, B. Guizal, S. Grafström, D. van Labeke, L.M.

Eng

► **To cite this version:**

J. Seidel, F.I Baida, L. Bischoff, B. Guizal, S. Grafström, et al.. Coupling between surface plasmon modes on metal films. *Physical Review B: Condensed Matter and Materials Physics (1998-2015)*, 2004, 69 (12), pp.121405. 10.1103/PhysRevB.69.121405 . hal-00097011

HAL Id: hal-00097011

<https://hal.science/hal-00097011>

Submitted on 19 Apr 2021

HAL is a multi-disciplinary open access archive for the deposit and dissemination of scientific research documents, whether they are published or not. The documents may come from teaching and research institutions in France or abroad, or from public or private research centers.

L'archive ouverte pluridisciplinaire **HAL**, est destinée au dépôt et à la diffusion de documents scientifiques de niveau recherche, publiés ou non, émanant des établissements d'enseignement et de recherche français ou étrangers, des laboratoires publics ou privés.

Coupling between surface plasmon modes on metal films

J. Seidel,¹ F. I. Baida,² L. Bischoff,³ B. Guizal,² S. Grafström,¹ D. Van Labeke,² and L. M. Eng¹

¹*Institute of Applied Photophysics, University of Technology Dresden, D-01062 Dresden, Germany*

²*Laboratoire d'Optique P.M. Duffieux, Centre National de La Recherche Scientifique, Unité Mixte de Recherche 6603, Université de Franche-Comté, F-25030 Besançon Cedex, France*

³*Research Center Rossendorf, Institute of Ion Beam Physics and Materials Research, D-01314 Dresden, Germany*

(Received 18 December 2003; published 15 March 2004)

Using scanning near-field optical microscopy for probing surface plasmon fields, we show that energy can be transferred from the plasmon propagating on one interface to the mode bound to the other interface of a thin metal film. This coupling is mediated by a narrow groove interrupting the silver film. Excitation of the second plasmon mode is detected by mapping the spatial intensity modulation induced by the interfering fields of the two plasmons. A quantitative analysis provides detailed knowledge about the degree of coupling. Our interpretation of the experimental results is confirmed by a numerical simulation of the field distribution.

DOI: 10.1103/PhysRevB.69.121405

PACS number(s): 73.20.Mf, 07.79.Fc

Surface plasmons (SP's) are surface-bound electromagnetic waves supported by metals due to the free-electron gas leading to a negative dielectric constant.¹ Recent years have seen a strong revival of the interest in such excitations, motivated by the possibility they offer for realizing a strong spatial confinement of electromagnetic fields.^{2–9} It is now widely expected that SP's will play an important role in future integrated nano-optical devices.

The most elementary SP is a SP propagating along the flat interface between a metallic and a dielectric half space. The plasmon field decays exponentially as an evanescent wave in the direction normal to the interface both into the metal and into the dielectric (with different decay lengths) and, hence, does not couple to any freely propagating electromagnetic mode (this means that it cannot be excited by light impinging on the interface). In the case of a metal film bounded by two dielectrics, there are two plasmon modes. As long as the film is not too thin, each mode can be assigned to one of the interfaces, where its field is concentrated. The situation remains similar to the former case, each mode being characterized by evanescent waves on both sides of the respective interface. The field of the plasmon localized at one interface decays across the metal film and a small residual field extends across the other interface into the second dielectric. However, provided that this is the dielectric with the higher index of refraction, the field may now become propagating rather than remaining evanescent. This is the effect used in the Kretschmann-Raether configuration for exciting SP's by light:¹ A metal film is bounded by air on one side and by a glass substrate on the other side. The SP at the metal-air interface couples weakly to a freely propagating mode in the glass. Hence, the SP can now be excited by light incident from the glass side at a specific angle (always lying in the range of total internal reflection). At the same time, the SP now suffers from radiative loss and is therefore more strongly damped. The SP at the metal-glass interface, however, remains decoupled from any freely propagating light wave.

Recently, Sönnichsen *et al.*¹⁰ and Thio *et al.*¹¹ showed that the energy of SP's excited on one side of a metal film, either by the tip of a scanning near-field optical microscope

(SNOM) or via a surface grating, can be transferred to the other side and radiated there via subwavelength holes in the film. In the present Rapid Communication, we show that a single groove in a silver film can couple energy from the upper SP mode to the nonradiative lower one. The excitation of the lower mode is directly detected with a SNOM as an intensity modulation due to spatial beating between SP modes. For a quantitative analysis we use the formulas describing SP's on the surface of a metal halfspace. They provide a good approximation also for films in the thickness range used in our experiment. However, the radiative damping of the upper mode has to be taken into account additionally, as well as the modification of the field of the lower mode close to the film surface where the field is probed. The image contrast can be understood quantitatively and we determine the mode coupling efficiency. We also show in a numerical simulation how the groove gives rise to such a coupling.

Our experiment uses the Kretschmann-Raether configuration for exciting the upper SP on a silver film on glass (BK7) by a focused (spot size $10 \times 15 \mu\text{m}^2$) *p*-polarized He-Ne laser beam ($\lambda = 632.8 \text{ nm}$). The excited SP propagates along the metal surface, which at a distance of 35–50 μm from the focus is intersected by a 490 nm wide groove at right angle to the direction of SP propagation. A dielectric fiber tip serving as a near-field probe is approached to the silver surface, the distance being controlled by shear-force detection.¹² The tip acts as a local scattering center, thereby converting the plasmon field to a propagating electromagnetic wave traveling down the optical fiber to a photodiode. Only bare dielectric fiber tips without any metal coating were used in order to prevent strong field distortions by the tip. Silver films of 60 nm thickness were prepared by thermal evaporation in vacuum ($p < 10^{-6}$ mbar) at high evaporation rates ($\sim 10 \text{ nm/s}$). Straight grooves in the silver film were produced by focused-ion-beam structuring using the improved IMSA system¹³ equipped with the high-resolution ion-optical column CANION 31Mplus (Orsay Physics). Within the grooves the silver was removed completely down to the bare glass substrate.

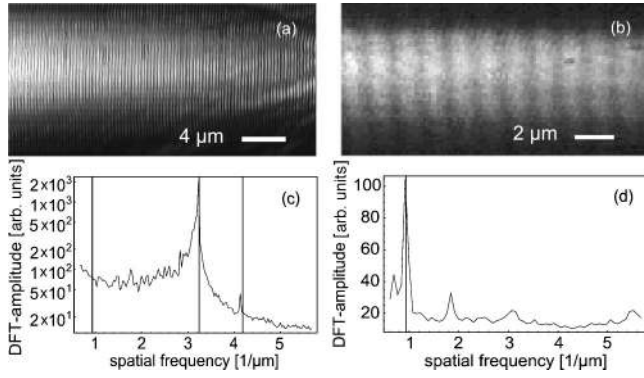


FIG. 1. Near-field images of the plasmon intensity before (a) and after (b) the groove. The incident plasmon propagates from left to right. The groove is situated outside the displayed areas close to the right, respectively, left border. The two images were taken in different runs at different locations along the groove. (c) and (d): Fourier transforms of (a) and (b). Vertical lines indicate the calculated beating modes. Note the logarithmic ordinate in (c).

The most striking features in the near-field images, obtained by scanning the tip across the surface close to the groove, are a short-wavelength standing-wave pattern in the upstream area [Fig. 1(a)] and a similar pattern with a much larger period in the region beyond the groove [Fig. 1(b)]. The pattern in Fig. 1(a) is readily explained by reflection of the incident wave (k vector $k_i=k$) at the groove leading to a counter-propagating wave ($k_r=-k$). The superposition of the two waves results in a stationary spatial intensity modulation with period $\Lambda_1=2\pi/|k_i-k_r|=\pi/k$. The theoretical value of k follows from the dispersion relation of the SP:¹

$$k = \frac{\omega}{c} \sqrt{\frac{\epsilon_{mr}\epsilon_d}{\epsilon_{mr} + \epsilon_d}}, \quad (1)$$

where $\omega/(2\pi)$ denotes the frequency, ϵ_{mr} is the real part of the dielectric constant of the metal, and ϵ_d is the dielectric constant of the adjacent dielectric medium. With $\epsilon_{mr}=-17.9$ (Ref. 14), $\epsilon_d=1$, and $\omega/c=2\pi/(632.8\text{ nm})$ we obtain $k=2\pi/(614.8\text{ nm})$. Hence, we expect a period of the standing-wave pattern of $\Lambda_1=307.4\text{ nm}$. For determining an accurate experimental value, each line of the SNOM image was Fourier transformed and the average amplitude spectrum was calculated as shown in Fig. 1(c). The spectrum is dominated by a narrow peak corresponding to a wavelength of 310 nm, which is very close to the theoretical expectation.

The occurrence of a standing wave after the groove [Fig. 1(b)] might be surprising at first sight, as only a transmitted wave should exist on that side with no back propagation. However, the groove breaks the translational invariance along the direction of plasmon propagation and therefore the k vector is no longer a preserved quantity. Hence, in the process of transmission and reflection, also the SP at the metal-glass interface may be excited. The wave number of this SP mode is $k'=2\pi/(390\text{ nm})$ as obtained from Eq. (1) with $\epsilon_d'=n^2$, $n=1.515$ being the refractive index of the glass substrate.

Consequently, two SP's, one at each interface, propagate away from the groove. The evanescent electromagnetic field of the SP at the lower interface extends across the metal film and leaks into the air space above the film, where it is superimposed on the field of the SP at the top interface. The interference of these two transmitted fields, oscillating at the same frequency but propagating with different k vectors $k_t=k$ and $k_t'=k'$, leads to the formation of the standing intensity pattern recorded by the SNOM. The modulation period is given by $\Lambda_2=2\pi/|k_t-k_t'|=1.06\text{ }\mu\text{m}$, again in agreement with the experimental value of $1.09\text{ }\mu\text{m}$ deduced from the Fourier spectrum [Fig. 1(d)].

At the groove, the lower SP mode should be excited not only in the forward direction, but such a wave should also emanate backwards into the upstream region. Thus, in the area imaged in Fig. 1(a), three waves are expected to interfere with each other: the incident ($k_i=k$) and reflected ($k_r=-k$) SP's at the surface and a reflected SP ($k_r'=-k'$) at the inner interface. The existence of the third wave gives rise to two additional fringe periods besides Λ_1 : $\Lambda_2=2\pi/|k_r-k_r'|=1.06\text{ }\mu\text{m}$ (identical with the period after the groove) and $\Lambda_3=2\pi/|k_i-k_r'|=239\text{ nm}$. However, only one of these two spatial frequencies appears as a clear narrow line in the experimental Fourier spectrum [Fig. 1(c)]. This line, representing a period of 242 nm close to the predicted value of Λ_3 , is two orders of magnitude smaller in amplitude than the peak at $1/\Lambda_1$. The missing third peak arises from beating between the two reflected SP's (i.e., the two weakest of the three fields) and may therefore easily be lost in the noise (see below).

The visibility of the beating patterns allows us to estimate quantitatively the reflection coefficient and the efficiency of the coupling between the two plasmon modes. It appears reasonable to assume that the radiation of energy from the tip into the optical fiber is mainly due to the electric-field component along the sample surface, i.e., in the direction of plasmon propagation (x axis). This assumption is supported by theory,¹⁵ but is still subject to some debate.¹⁶ Therefore, let E_{xi} , E_{xr} , and E'_{xr} be the respective field amplitudes of the incident, reflected upper, and reflected lower SP's close to the metal surface at the groove edge, situated at $x=0$. Then, in the upstream region ($x<0$) the x component of the total field can be written as

$$E_x(x,t) = (E_{xi}e^{-\kappa x}e^{ikx} + E_{xr}e^{\kappa x}e^{-i(kx+\phi)} + E'_{xr}e^{\kappa'x}e^{-i(k'x+\phi')})e^{-i\omega t}, \quad (2)$$

where κ and κ' denote the damping constants of the two plasmon modes, and ϕ and ϕ' account for possible phase shifts upon reflection. The damping is due to internal damping in the metal (described by the imaginary part ϵ_{mi} of its dielectric constant, $\epsilon_{mi}=0.7$ for silver at $\lambda=632.8\text{ nm}$)¹⁴

$$\kappa = \frac{\omega}{c} \left(\frac{\epsilon_{mr}\epsilon_d}{\epsilon_{mr} + \epsilon_d} \right)^{3/2} \frac{\epsilon_{mi}}{2\epsilon_{mr}^2}, \quad (3)$$

which yields $\kappa=(85\text{ }\mu\text{m})^{-1}$ and $\kappa'=(22\text{ }\mu\text{m})^{-1}$. The upper SP is additionally subject to radiative loss to the glass

substrate, which gives a corrected value of $\kappa=(59 \mu\text{m})^{-1}$ for a 60 nm thick silver film.¹ This value is in good agreement with the intensity decay length of somewhat less than 30 μm observed in our SNOM images. From Eq. (3) the time-averaged intensity associated with E_x follows as

$$|E_x|^2 = E_{xi}^2 e^{-2\kappa x} + E_{xr}^2 e^{2\kappa x} + E_{xr}'^2 e^{2\kappa' x} + 2E_{xi}E_{xr} \cos(2kx + \phi) + 2E_{xr}E_{xr}' e^{(\kappa'+\kappa)x} \cos[(k'-k)x + \phi' - \phi] + 2E_{xi}E_{xr}' e^{(\kappa'-\kappa)x} \cos[(k'+k)x + \phi']. \quad (4)$$

The average intensities are given by the first three terms, followed by the three beating signals with wave numbers $2k$, $k'-k$, and $k'+k$ corresponding to the periods Λ_1 , Λ_2 , and Λ_3 defined earlier. The amplitude of the dominating modulation at $2k$ is independent of x (as indeed confirmed by the experiment), whereas the other two modulations decay away from the groove with different decay constants $\kappa'+\kappa=(16 \mu\text{m})^{-1}$ and $\kappa'-\kappa=(35 \mu\text{m})^{-1}$.

The visibility $v=2E_{xi}E_{xr}/(E_{xi}^2+E_{xr}^2+E_{xr}'^2)$ of the dominant interference pattern close to the groove ($x=0$) can be determined directly from single line scans taken from the SNOM image and is found to be roughly $v=0.8$. With $E_{xr}'^2 \ll E_{xi}^2$ it follows that $E_{xr}=0.5E_{xi}$, which means that 25% of the intensity is reflected in the upper mode in the present case.

From the Fourier spectrum in Fig. 1(c) we deduce that the intensity pattern at $k'+k$ (Λ_3) is weaker by a factor of ~ 100 , hence $E_{xr}'=0.01E_{xr}$ according to Eq. (4). The field of the lower mode at the inner interface is connected with the field at the surface mainly by an exponential factor determined by the decay constant $\alpha'_m=[k'^2-\epsilon_{mr}(\omega/c)^2]^{1/2}$ of the evanescent field in the metal. For a film thickness $d=60$ nm we obtain a factor $\exp(-\alpha'_m d)=1/15$. However, the field is modified by the presence of the metal-air interface, and this causes a deviation by a factor $\beta'=2\epsilon_{mr}\alpha'_d/(\epsilon_{mr}\alpha'_d+\epsilon_d\alpha'_m)$, where α'_d is the transverse decay constant of the lower mode in the upper dielectric, which is obtained from the same formula as α'_m with ϵ_{mr} replaced by $\epsilon_d=1$. Here $\beta'=2.5$, so that the field at the inner interface is $\tilde{E}'_{xr}=6E'_{xr}=0.03E_{xi}$. By integration of the Poynting vector of a weakly damped SP with field amplitude E_x , bound to the interface between two media with dielectric constants ϵ_d and ϵ_{mr} , one can easily show that the total-energy flux along the direction of propagation is proportional to $E_x^2(\epsilon_d+\epsilon_{mr})^2(\epsilon_d-\epsilon_{mr})/(-\epsilon_{mr}\epsilon_d)^{3/2}$. With this, the factor of 0.03 in the field transforms to 2.4×10^{-4} in the energy flux, which means that only a very small fraction of the power is transferred to the lower reflected mode.

Due to $E_{xr}=0.5E_{xi}$, the contribution at $k'-k$ should be weaker than the pattern at $k'+k$ by a factor of two. Furthermore, the stronger damping of this signal leads to a broadening of the spectral line at the expense of a reduced peak height. This and the fact that the noise level is relatively high in the interesting wave-number region (probably due to diffuse scattering of the incident wave at irregularities of the groove edge) explains why we did not succeed to resolve this

line. However, this beating mode, produced by upper and lower SP's propagating in the same direction, can be studied in detail after the groove, where it is clearly resolved [Fig. 1(b)]. A calculation for this region in the same spirit as above yields

$$|E_x|^2 = E_{xt}^2 e^{-2\kappa x} + E_{xt}'^2 e^{-2\kappa' x} + 2E_{xt}E_{xt}' e^{-(\kappa'+\kappa)x} \times \cos[(k'-k)x + \theta], \quad (5)$$

where E_{xt} and E_{xt}' are the respective field amplitudes of the two waves and θ is their mutual phase shift. A closer analysis of the image displayed in Fig. 1(b) clearly shows that the fringe pattern decays faster than the average intensity, in good quantitative agreement with the predicted decay lengths of 16 μm and 30 μm , respectively. The visibility of the interference pattern close to the groove is $v \approx 0.3$, which yields $E_{xt}' \approx 0.15E_{xt}$. Thus, the field at the inner interface $\tilde{E}'_{xt}=6E'_{xt}=0.9E_{xt}$ is almost as strong as the field at the surface. In terms of energy flux the ratio is 0.21. From a comparison of the intensities before and after the groove at the given location, we estimate that 55% of the incident power was transmitted across the groove to the upper mode. Hence, $0.21 \times 55\% = 12\%$ were coupled to the lower mode, indicating a rather efficient excitation. However, the efficiency seems to depend in a sensitive way on the detailed structure of the groove edges. When the plasmon excitation is moved to a different place along the groove, the visibility of the various interference patterns exhibits clear variations. Note that for display in Fig. 1 we chose images taken at different locations, showing the clearest patterns.

To gain more insight into the mode coupling introduced by the groove we performed model calculations using the finite-difference time-domain (FDTD) method, which allows both temporal and permanent responses to be studied.¹⁷ This method, which is rigorous, is more adapted for the study of a deep groove than the Rayleigh perturbative one used in Ref. 18. In order to account for the generation and propagation of the SP, we need to consider a large spatial domain of computation. The stability criteria stipulate that the spatial step width should be less than $\Delta^{limit}=\lambda/20$. However, in the present case, a finer mesh is needed to describe the metal layer and the groove correctly. In order to achieve a good representation of geometrical details while at the same time keeping the number of nodes within a reasonable limit we developed a FDTD code allowing a nonuniform discretization of the structure.¹⁷ The spatial meshing step is set to 5 nm for fine geometrical features and to 30 nm in other areas. To avoid large local errors (virtual reflections) due to an abrupt change of the step width between two domains, they must be separated by an intermediate domain where the spatial step varies slowly between the fine and the coarse mesh. Thus, our domain is meshed with only 4.2×10^5 nodes instead of 4×10^8 nodes, which would be necessary for a regular discretization. In addition, perfectly-matched-layer (PML) absorbing conditions (adapted to the nonuniform mesh) were used in order to cancel parasitic reflections at the boundaries of the FDTD window of computation.¹⁹

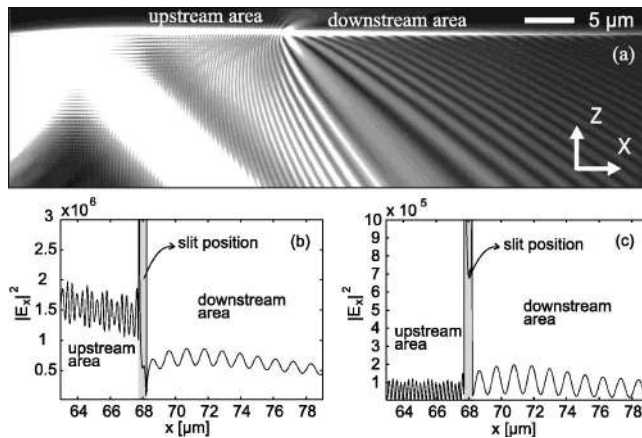


FIG. 2. (a) FDTD-calculated intensity distribution in the plane of incidence of the exciting laser beam in logarithmic gray scale; (b) and (c) cross sections in the region of a 490 nm wide groove, 5 nm above (air) and below (glass) the metal, respectively.

In the calculation, the thickness and optical constants of the silver film, the parameters of the exciting laser beam, and the groove width were set to the values specified above. The angle of incidence (42.81°) was chosen to give the most efficient SP excitation. Figure 2(a) shows the time-averaged intensity distribution of the electromagnetic field for the whole FDTD lattice. In Fig. 2(b) a cross section taken 5 nm above the metal film across the slit is displayed, which is expected to reflect rather closely the experimentally mea-

sured quantity. The characteristic features observed experimentally are well reproduced: The reflection of the SP at the slit induces a fringe pattern with a period of 304 nm. In the downstream region a long-period standing-wave pattern is clearly visible with a period of $1.08 \mu\text{m}$. The role of the lower SP mode becomes evident upon inspection of the intensity close to the lower interface [Fig. 2(c)], which is not accessible experimentally. Here, in the downstream region the long-period pattern exhibits an increased visibility, while in the upstream region the pattern is now dominated by a modulation period of 240 nm, produced by the interference of the lower reflected mode with the incident upper one. A quantitative comparison with the experiment with respect to the coupling efficiency is not meaningful at present, as the experiment clearly indicates a strong dependence on geometrical details. This will be a subject of future investigations.

In conclusion, we have shown that a straight groove in a metal film causes the two plasmon modes at the two film boundaries to exchange energy and that this coupling can be rather pronounced. SNOM provides a unique tool for studying this phenomenon by analyzing the standing-wave patterns created by the interfering plasmon modes, which allowed us to deduce the coupling efficiency. The detailed theoretical modeling based on the FDTD method offers the prospect of gaining an improved understanding of the coupling process and its dependence on various parameters. Plasmon mode coupling may become an important building block in plasmon-based nano-optical signal processing.

- ¹H. Raether, *Surface Plasmons on Smooth and Rough Surfaces and on Gratings* (Springer, Berlin, 1988).
- ²B. Hecht, H. Bielefeldt, L. Novotny, Y. Inouye, and D.W. Pohl, *Phys. Rev. Lett.* **77**, 1889 (1996).
- ³I.I. Smolyaninov, D.L. Mazzoni, J. Mait, and C.C. Davis, *Phys. Rev. B* **56**, 1601 (1997).
- ⁴J.-C. Weeber, C. Girard, J.R. Krenn, A. Dereux, and J.-P. Goudonnet, *J. Appl. Phys.* **86**, 2576 (1999).
- ⁵A. Bouhelier, T. Huser, H. Tamaru, H.-J. Güntherodt, D.W. Pohl, F.I. Baida, and D. Van Labeke, *Phys. Rev. B* **63**, 155404 (2001).
- ⁶J.-C. Weeber, J.R. Krenn, A. Dereux, B. Lamprecht, Y. Lacroute, and J.P. Goudonnet, *Phys. Rev. B* **64**, 045411 (2001).
- ⁷P. Dawson, B.A.F. Puygranier, and J.-P. Goudonnet, *Phys. Rev. B* **63**, 205410 (2001).
- ⁸S.I. Bozhevolnyi, J. Erland, K. Leosson, P.M.W. Skovgaard, and J.M. Hvam, *Phys. Rev. Lett.* **86**, 3008 (2001).
- ⁹W.L. Barnes, A. Dereux, and T.W. Ebbesen, *Nature (London)* **424**, 825 (2003).
- ¹⁰C. Sönnichsen, A.C. Duch, G. Steininger, M. Koch, G. v. Plessen,

- and J. Feldmann, *Appl. Phys. Lett.* **76**, 140 (2000).
- ¹¹T. Thio, K.M. Pellerin, R.A. Linke, H.J. Lezec, and T.W. Ebbesen, *Opt. Lett.* **26**, 1972 (2001).
- ¹²J. Seidel, S. Grafström, L. Eng, and L. Bischoff, *Appl. Phys. Lett.* **83**, 1368 (2003).
- ¹³L. Bischoff, J. Teichert, E. Hesse, D. Panknin, and W. Skorupa, *J. Vac. Sci. Technol. B* **12**, 3523 (1994).
- ¹⁴U. Schröder, *Surf. Sci.* **102**, 118 (1981).
- ¹⁵D. Van Labeke and D. Barchiesi, *J. Opt. Soc. Am. A* **10**, 2193 (1993).
- ¹⁶A. Dereux, C. Girard, and J.-C. Weeber, *J. Chem. Phys.* **112**, 7775 (2000).
- ¹⁷A. Taflove and S. Hagness, *Computational Electrodynamics: The Finite-Difference Time-Domain Method*, 2nd ed. (Artech House, Boston, 2000).
- ¹⁸F.I. Baida, D. Van Labeke, and J.-M. Vigoureux, *Phys. Rev. B* **60**, 7812 (1999).
- ¹⁹J.-P. Berenger, *J. Comput. Phys.* **114**, 185 (1994).